

Physical modeling of soil arching around shallow tunnels in sandy grounds

Nader Moussaei ^a, Mohammad Hossein Khosravi ^{a,*}, Mohammad Farouq Hossaini ^b

^a School of Mining Engineering, College of Engineering, University of Tehran, Tehran, Iran.

^b School of Minerals and Energy Resources Engineering, UNSW, Sydney, Australia.

Article History:

Received: 16 January 2022.

Revised: 14 June 2022.

Accepted: 21 June 2022.

ABSTRACT

The distribution of earth pressure surrounding a tunnel is one of the most critical factors in designing tunnel support systems. In this study, a physical modeling setup has been designed and constructed to simulate the excavation procedure of a full-face circular tunnel. Silica sand was used with four different densities and three different cover-to-tunnel diameter ratios. The full-face excavation was simulated with a variation of tunneling-induced volume loss. The variations of earth pressure around the tunnel were measured by means of a series of miniature soil pressure cells. Particle Image Velocimetry (PIV), as a non-destructive image processing technique, was used to monitor the deformation of the soil surrounding the tunnel. The results obtained from both pressure cells and PIV showed that soil arching developed around the tunnel. As tunnel convergence increased, a loosened zone appeared above the tunnel, surrounded by a stress arch. It was discovered that there is a direct relationship between the height of the loosened zone and the depth of the tunnel. A linear equation has been established for the estimation of the height of the loosened zone, which has a direct influence on the design of the support system.

Keywords: Tunneling; Physical model; Soil arching; Particle Image Velocimetry (PIV).

1. Introduction

Excavation of an underground opening leads to disturbance of the in-situ stresses around the opening, resulting in a redistribution of surrounding stresses. The matter of stress redistribution around an excavated opening is a key factor in stability analysis and support system design. The governing phenomenon in stress redistribution around sandy shallow tunnels is soil arching. The pioneer in soil arching investigation was Janssen (1895), who observed a non-hydrostatic vertical pressure distribution in granular material stored in silos. Terzaghi (1936) investigated the soil arching effect by means of some trap door tests. He concluded that by moving the trap door down, the weight of the backfill transferred from the yielding zone above the door to the surrounding stationary zones. This phenomenon was observed in some other geotechnical projects such as pipeline ditches (Marston and Anderson 1913), retaining walls (Terzaghi 1934; Krynine 1945; Handy 1985; Khosravi et al. 2013), and undercut slopes (Khosravi et al. 2011; Khosravi et al. 2016). Balla (1963) calculated the rock pressure by considering shearing resistance. Yang et al. (2013) introduced the analytical method based on the non-linear Mohr-Coulomb criteria to measure supporting pressure on the quadrilateral tunnel. They used the modified tangential technique, the upper solution of supporting pressure for the shallow tunnel. They investigated the effect of lateral pressure coefficient, initial cohesion, uniaxial tension strength, overburden, and tunnel span. Fraldi et al. (2010) measured the collapsed zone area using the plasticity theory. They calculated the extension of the collapsed zone by the associated flow rule and defined the plastic potential function coinciding with the Hoek-Brown yield criterion. They then captured the geometry of the collapsed zone by considering the Greenberg Minimum Principle. Mollon et al. (2011) introduced a three-dimensional analytical method, a rotational failure mechanism to

predict face pressure. They believed that the boundary of the collapsed zone in front of the tunnel face consists of two logarithmic spirals. Ibrahim et al. (2015) extended this method to a layered ground with different friction angles. Similarly, Pan and Dias (2017) modified this method to cover non-circular tunnels.

Among analytical and experimental methods, there are several physical models conducted to investigate the supporting pressure. Lei et al. (2015) examined the effect of the dip of the ground surface on the supporting pressure. They built and tested a 1-g physical model with three different surface dip angles. They excavated the tunnel section in several steps and recorded the amount of strain on the tunnel lining as well as applied pressure on it. Chen et al. (2013) conducted a physical model to measure the tunnel face pressure and they did the test for three cover-to-tunnel diameter ratios. They simulated mechanized tunnel excavation using a three-dimensional model. The tunnel face consisted of a rigid circular plate connected to a hydraulic jack that was capable of pushing back the face at a low rate. Moreover, they recorded the variation of pressure during displacement of the tunnel face. They defined vertical and horizontal stress concentration coefficients. Based on the outcomes recorded by pressure cells, buried around the tunnel, they obtained the loosened zone, arch crown, and arch foot through the amount of the previously mentioned coefficient.

The effect of tunnel overburden and in-situ stress coefficient was investigated by Chen et al. (2011) using a numerical method. They drew the variation of the vertical stress over depth during the progress of the tunnel face to the measuring point. Based on these diagrams, they defined the height of the loosened zone above the tunnel. Zhang et al. (2015) simulated a three-dimensional numerical model representative of the ground with four different geologies. They tried to find out the

* Corresponding author. E-mail address: mh.khosravi@ut.ac.ir (M. H. Khosravi).

variation of the tunnel face pressure over the tunnel face convergences. Besides these methods, Rezaei et al. (2017) used artificial neural network methodology to investigate the height of the distressed zone above mined panel in longwall mining.

Amongst all, tunneling-induced ground displacement is the most influential parameter affecting stress redistribution around a tunnel. Tunnel geometry, soil density, and overburden are, also, essential. Ground density and tunneling-induced ground displacement have rarely been taken into account in previous studies, particularly in physical models. In order to fill the gaps left in the previous studies, this research has been set up to investigate the ground movement in loose materials subjected to tunneling and to evaluate the influence of soil density on the tunnel supporting pressure. This investigation is based on a series of 1-g physical model tests. The modeling has been carried out under different cover-to-tunnel diameter ratios as well as different tunnel volume losses.

2. Physical Model Components

2.1. Model frame

A rigid model frame of 30 cm in width, 120 cm in length, and 145 cm in height were built using stainless steel beams. The components of the model frame are illustrated in Figure 1. During the test process, the mean deflection of the acrylic plate was less than 0.1 mm, which was 0.03 percent of the model width and 30 percent of the mean particle size of the used sand. Thus, the plates were believed to be sufficiently rigid for the study.



Figure 1. Physical model of the full-face tunnel excavation.

2.2. Modeling material

The Firuzkuh silica sand with a uniformity coefficient of 2.3 and a mean particle size of 0.3 mm was used as the modeling material. The particle size distribution of the sand is shown in Figure 2. The dry sand has an internal friction angle and cohesion of 36° and zero, respectively.

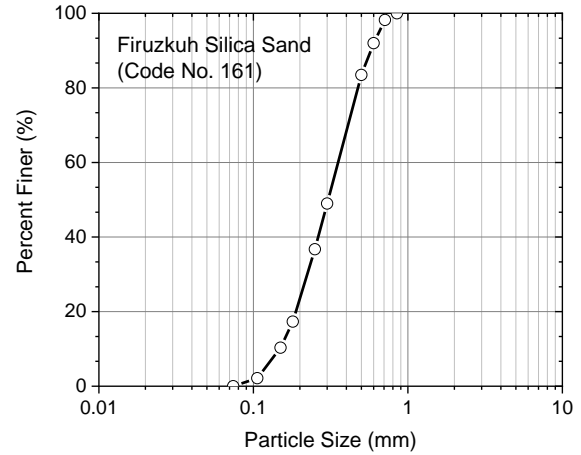


Figure 2. Particle size distribution of Firuzkuh silica sand No. 161.

2.3. Preparation of the model

The models were prepared using the sand pluviation method in which the sand particles were poured from the feeder under a specific falling height, depending on the target density. The target densities of 1400, 1417, 1441, and 1482 kg/m³ were obtained from the falling heights of 10cm, 30cm, 60cm, and 110cm, respectively. The modeling process was repeated under the preceding mentioned densities for three different cover-to-tunnel diameter ratios (C/D) of 2, 3, and 4.

2.4. Pressure measurement procedure

Five pressure cells were used to measure the soil pressure variation around the tunnel while the volume loss increased (simulation of full-face excavations). Each pressure cell was calibrated by a loading-unloading process under hydrostatic water pressure as shown in Figure 3.

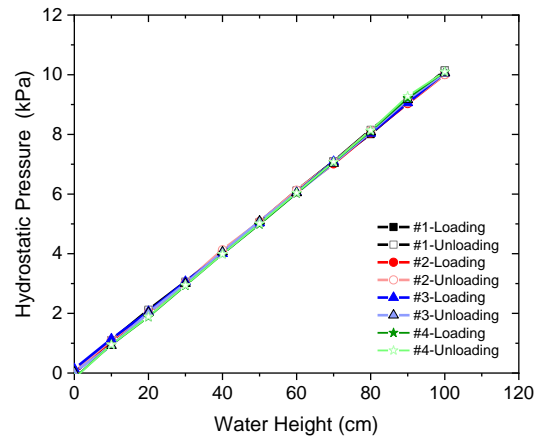


Figure 3. Calibration of the procedure cells in water.

The application of pressure cells in soil was validated under a series of loading-unloading processes as represented in Figure 4. For this validation, the pressure cells were placed at the bottom of the container and the process of loading-unloading was conducted by pouring the sand through the sand feeder and gathering it by a suction machine.

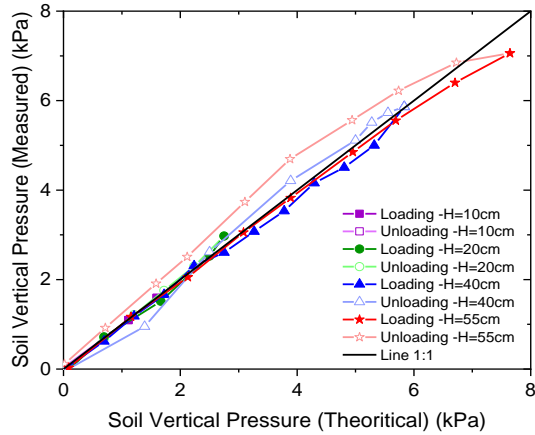


Figure 4. Validation of the application of pressure cells in soil.

The results indicated that as the soil height increased, the measured soil pressure, during the unloading process, was less than the theoretically expected values. This phenomenon is due to the side friction, known as the silo effect (Janssen 1895). To avoid the influence of this phenomenon on the results, the depth of the pressure cells, inside the model, was kept limited. Three of the pressure cells were used to monitor the vertical soil pressure variation above the tunnel, and one of them was to record vertical soil pressure variation at the tunnel level. The last one was used to monitor the horizontal soil pressure variation above the tunnel. The layout of the pressure cells inside the model is illustrated in Figure 5.

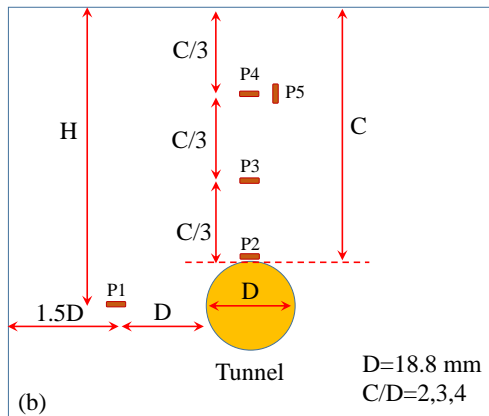
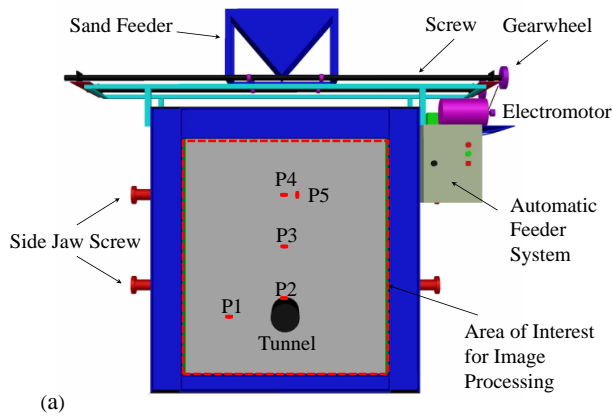


Figure 5. Soil pressure cell layout, (a) Physical model, (b) Sensor position.

2.5. Excavation Process

Full-face tunneling makes a uniform convergence around the tunnel in sandy soils. Full-face tunnel excavation was simulated through a pack of conic wedges, as shown in Figure 6. The tunnel diameter can be decreased by drawing out the inner conic wedge. Some researchers have employed this methodology for simulating the tunnel excavation process (Katoh et al., 1998; Boonsiri & Takemura, 2015).

As shown in Figure 6, a permanent magnet step motor was used to control the tunnel convergence with no vibration. The initial tunnel diameter of 188 mm was reduced to 174 mm, under a constant convergence speed of 1.3 mm/min. As the factor of length scale was 50, the tunnel simulated in this study was representative of a tunnel with a diameter of 9.4 m in prototype (a common two-lane metro tunnel).

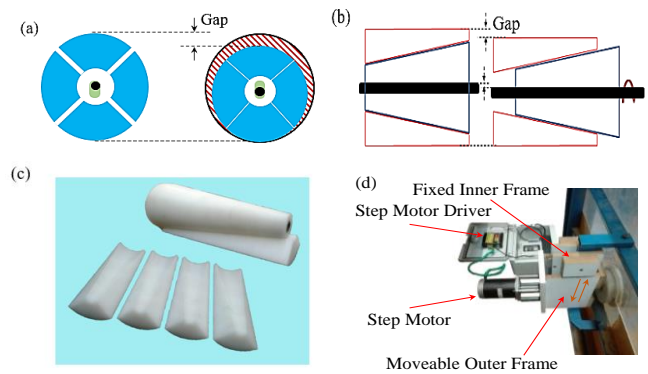


Figure 6. Full face excavation simulation procedure, (a) Front view, (b) Side view, (c) Tunnel conical parts, (d) Excavation simulator components.

2.6. Image Processing

The particle Image Velocimetry (PIV) technique was used to measure deformation contours in the model. This technique is approved worldwide as a non-destructive process. Moreover, it is used for the estimation of deformation under both centrifugal (Marshall et al., 2012) and 1-g conditions (Kirsch, 2010; Khosravi et al., 2011; Khosravi et al., 2013; Moussaei et al., 2016; Moussaei et al. 2018; Moussaei et al., 2019).

A PIV camera was placed at a 1.5-meter-distance, perpendicular to the model frame, as shown in Figure 7. A black curtain was hung behind the camera to avoid reflection of the screen light and to get a higher resolution. MatPIV v.1.6.1 computer code, developed by Sveen (2004), was utilized for analysis.

3. Results and Discussion

The gap parameter (the tunnel volume loss), sand density, and cover-to-tunnel diameter ratio were considered the governing parameters in this research. To study the influence of these parameters on the stress arching around the tunnel, a total number of 11 model tests were conducted, as listed in Table 1.

3.1. Soil pressure variation

Variation of soil pressure above the tunnel was recorded during tunnel convergence. Earth pressure around the tunnel, as a function of volume loss, is presented in Figures 8-10 for cover to tunnel diameter ratios of 2, 3, and 4, respectively. Pressure cell positions are shown in Figure 5. It should be noted that all the pressure cells were measuring vertical earth pressure, except for P5 which was planned to record horizontal earth pressure.

At an overall glance, it can be seen that by increasing the convergence of the tunnel, the vertical earth pressure decreases above the tunnel (P2, P3, and P4), while increasing laterally (P1). This can be regarded as clear evidence of the soil arching phenomenon. Also, the gradual increment

of horizontal earth pressure above the tunnel (P5), in most of the models, confirms the occurrence of this phenomenon. As Figures 8-10 show, when the model got denser, the redistribution of earth pressures around the tunnel occurred faster and the final state of earth pressure distribution, surrounding the tunnel, reached relatively lower values of tunnel volume loss.

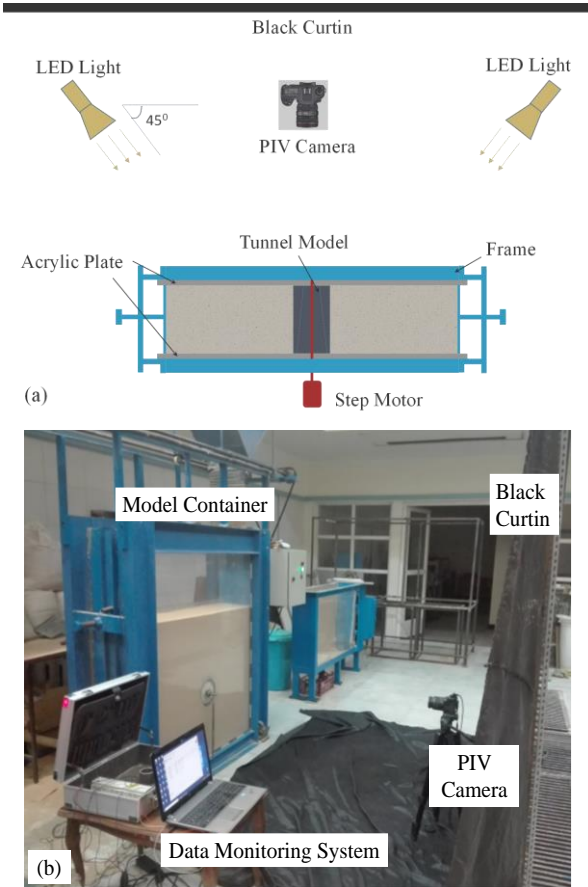


Figure 7. The photogrammetry setup, (a) Top view, (b) General view.

Table 1. The simulation parameters in physical models.

Model Test No.	Density, ρ (kg/m ³)	Cover-to-Tunnel Diameter Ratio, C/D
1		2
2	1400	3
3		4
4		2
5	1417	3
6		4
7		2
8	1441	3
9		2
10	1482	3
11		4

The distribution of vertical earth pressure above the tunnel, as a function of the tunnel volume loss, is shown in Figures 11-13 for different values of soil density and cover-to-diameter ratios. As the tunnel converged, the vertical earth pressure above the tunnel decreased all over. However, this decrement was maximum in close vicinity of the tunnel. According to Chen et al (2011), the inflection point in vertical earth pressure distribution curves can be considered as the crown of the loosened zone above the tunnel. The inflection points are marked with

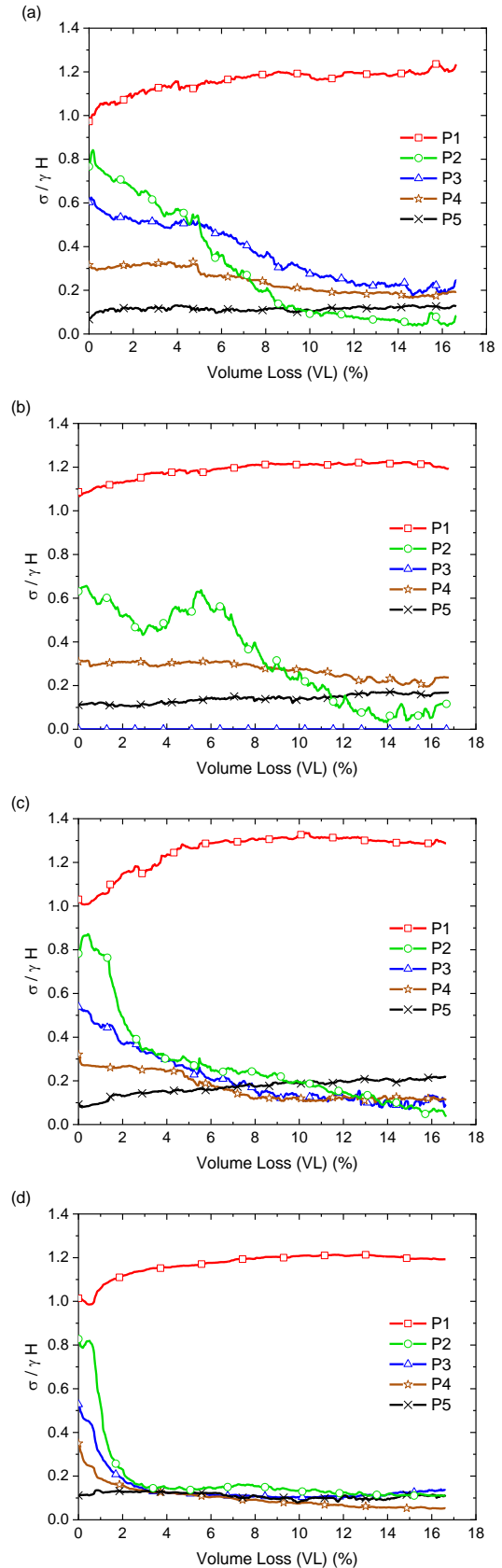


Figure 8. Distribution of earth pressure around the tunnel as a function of tunnel volume loss.

(C/D=2); (a) ρ =1398, (b) ρ =1417, (c) ρ =1441, (d) ρ =1482 kg/m³.

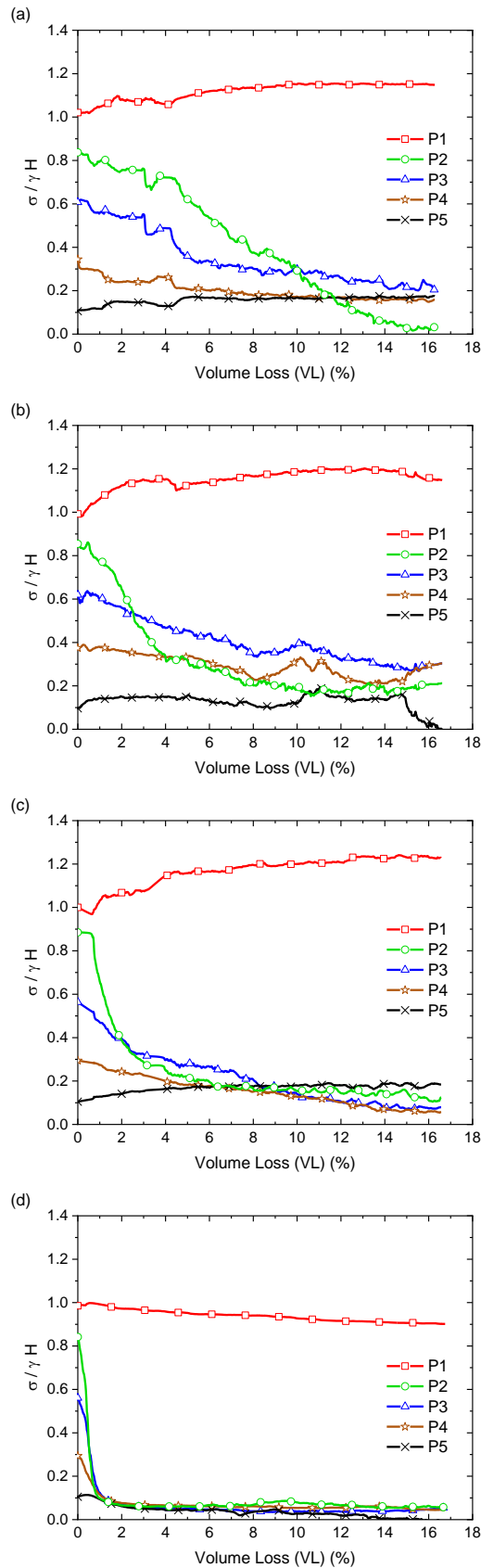


Figure 9. Distribution of earth pressure around the tunnel as a function of tunnel volume loss ($C/D=3$); (a) $\rho=1398$, (b) $\rho=1417$, (c) $\rho=1441$, (d) $\rho=1482$ kg/m^3 .

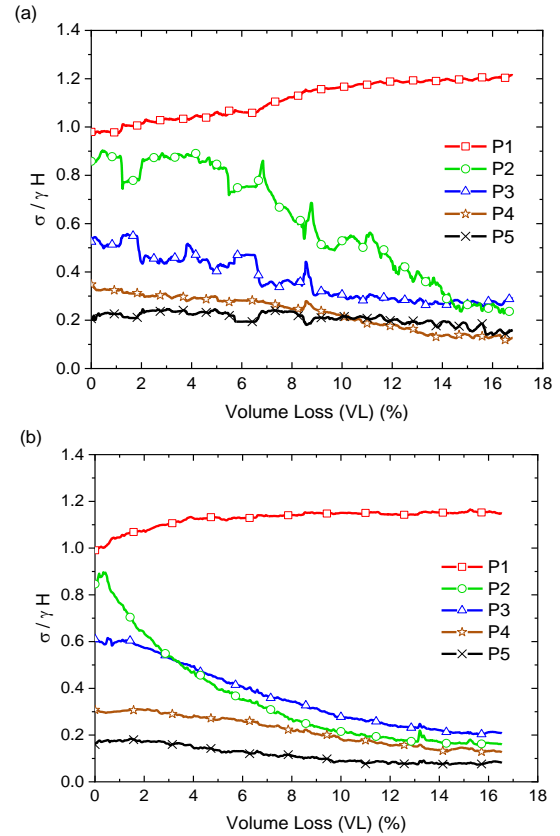


Figure 10. Distribution of earth pressure around the tunnel as a function of tunnel volume loss ($C/D=4$); (a) $\rho=1398$, (b) $\rho=1417$ kg/m^3 .

black circles in Figures 11-13. The distance between the inflection point and the tunnel roof is defined as the height of the loosened zone (h), in this study. It can be perceived from these figures that h is in direct relationship with volume loss of the tunnel. In other words, by increasing the convergence of the tunnel, the loosened zone extended upward.

3.2. Deformation of the model

In order to investigate the influence of soil stress arching on the deformation of the model, the Particle Image Velocimetry (PIV) technique was used to monitor the deformation of the model during the tunneling process. Details of image processing are reported in Moussaei et al. (2019). The displacement field for a cover-to-tunnel diameter ratio of 3 is plotted in Figure 14.

Variation of the vertical settlement (S) over depth (Z) for different values of soil density and cover-to-diameter ratios is illustrated in Figure 15 to Figure 17, where both the settlement and depth values are normalized with the tunnel cover (C). For a density of 1417 kg/m^3 , regardless of cover to diameter ratio, the rate of settlement is constant at any depth above the tunnel. However, by increasing the soil density, especially for deeper tunnels (higher values of C/D for a constant D), there is a change in the rate of settlement, as indicated by black circles in Figure 15 to Figure 17. This change in settlement rate is related to the soil arching phenomenon as discussed in the following section.

3.3. Loosened zone geometry

As mentioned before, during the excavation of the tunnel, the convergence of the surrounding soil leads to the development of soil stress arching around the tunnel. Due to this phenomenon, the weight of the soil transfers partially from the moving zone, above the tunnel, to adjacent stationary zones. Therefore, a shear surface will be appearing between the moving zone and stationary zones on each side of the tunnel (Lin et al. 2019).

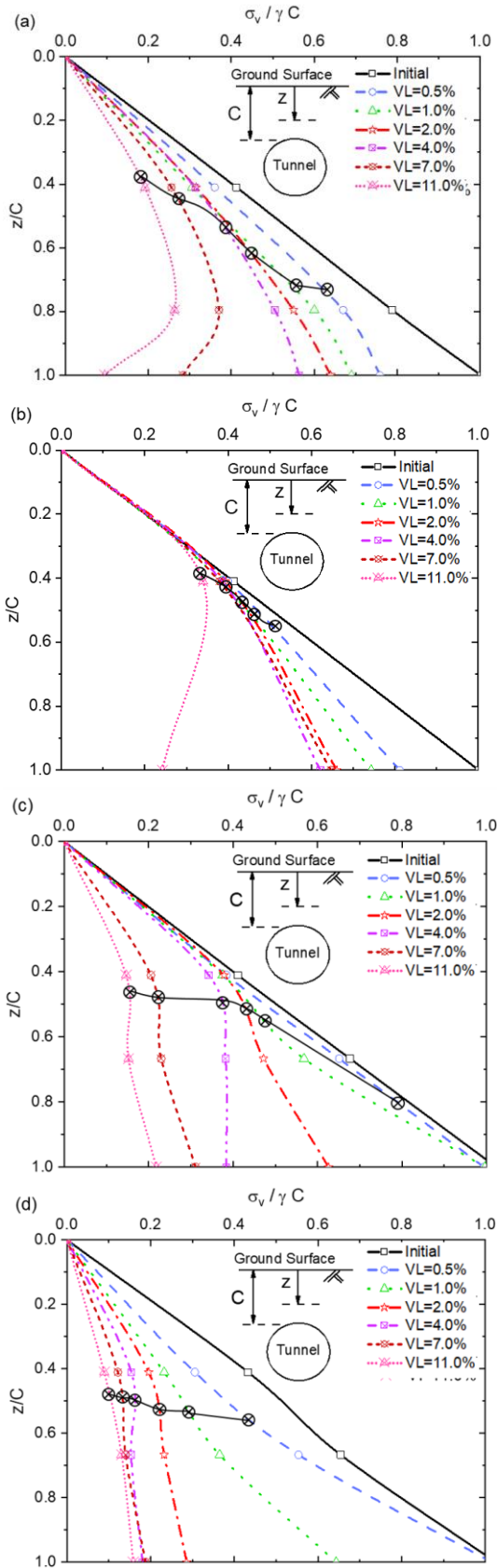


Figure 11. Distribution of vertical earth pressure above the tunnel as a function of tunnel volume loss.
(C/D=2); (a) $\rho = 1398$, (b) $\rho = 1417$, (c) $\rho = 1441$, (d) $\rho = 1482$ kg/m³.

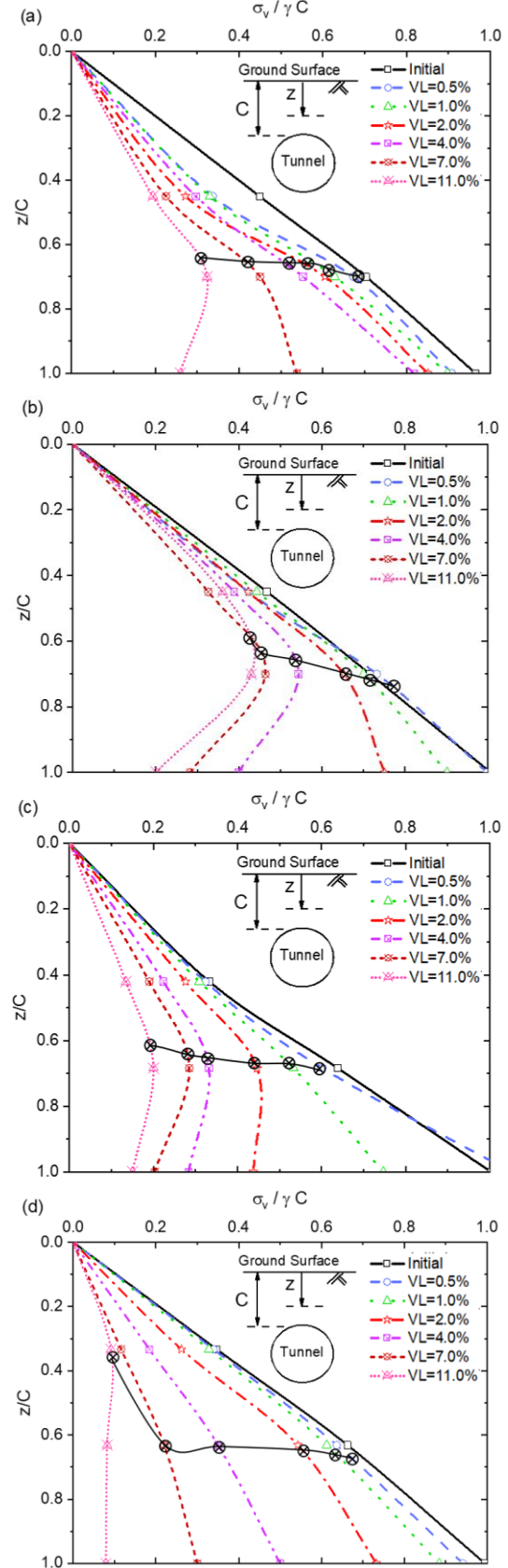


Figure 12. Distribution of vertical earth pressure above the tunnel as a function of tunnel volume loss.
(C/D=3); (a) $\rho = 1398$, (b) $\rho = 1417$, (c) $\rho = 1441$, (d) $\rho = 1482$ kg/m³.

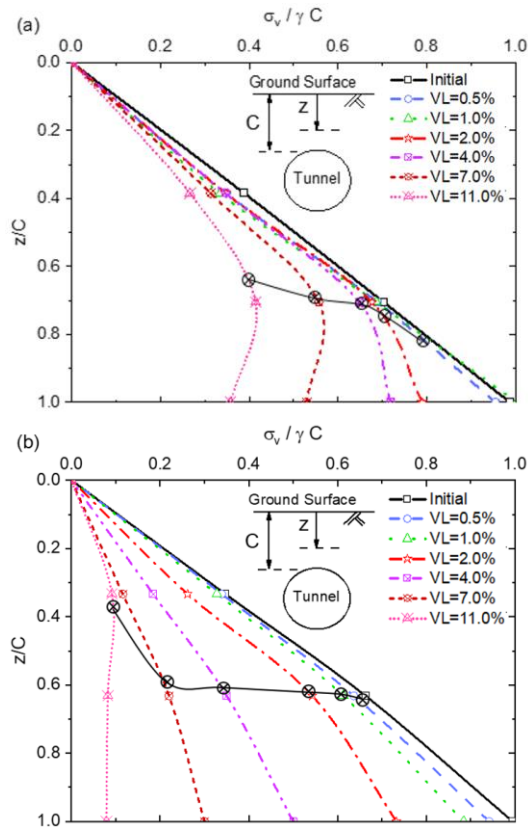


Figure 13. Distribution of vertical earth pressure above the tunnel as a function of tunnel volume loss. (C/D=4); (a) $\rho = 1398$, (b) $\rho = 1417 \text{ kg/m}^3$.

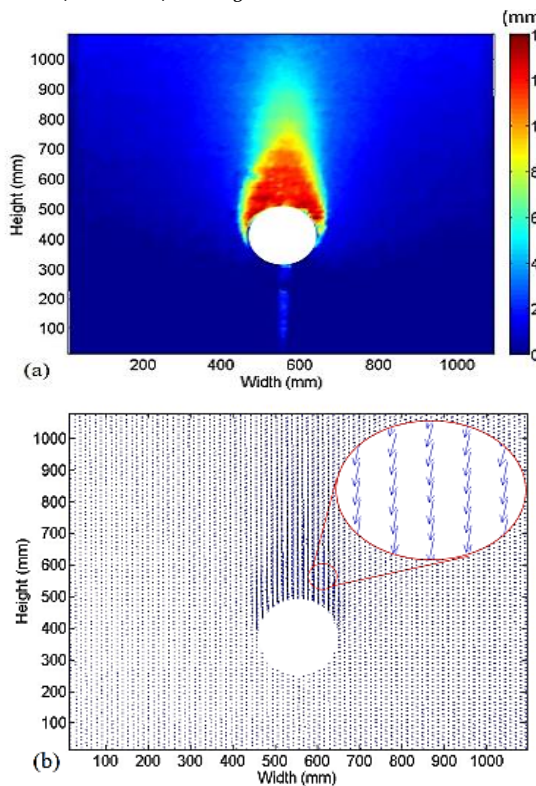


Figure 14. Displacement field for a cover-to-tunnel diameter ratio of C/D=3; (a) displacement contours, (b) displacement vectors.

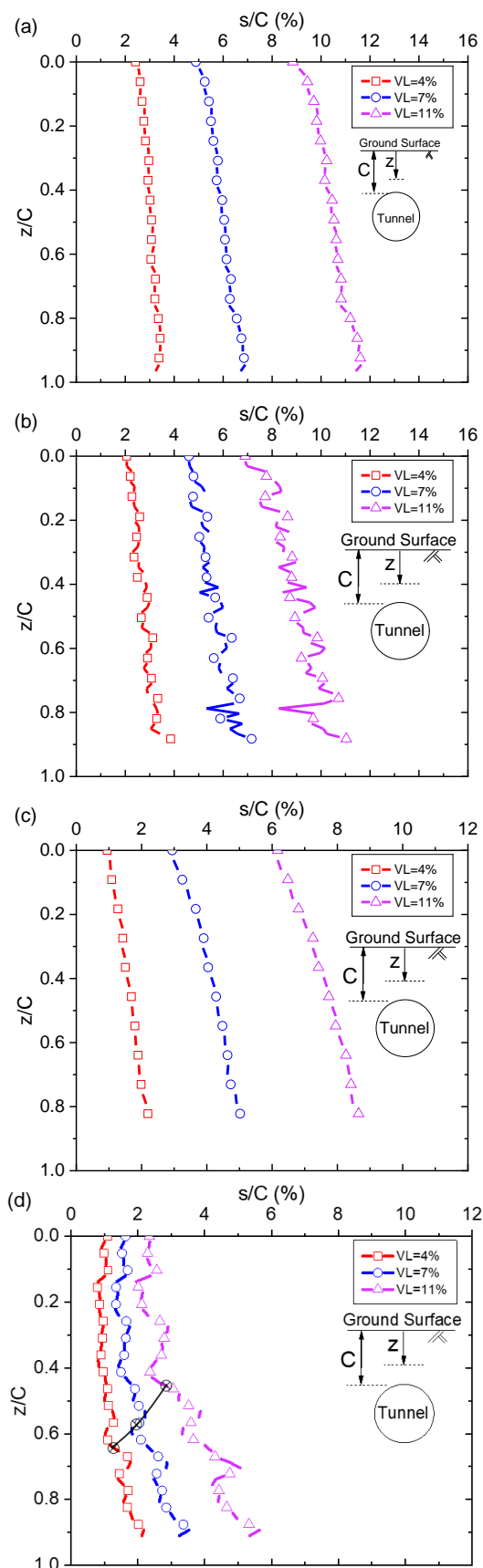


Figure 15. Variation of the vertical settlement above the tunnel crown for a cover-to-tunnel diameter ratio of C/D=2; (a) $\rho = 1398$, (b) $\rho = 1417$, (c) $\rho = 1441$, (d) $\rho = 1482 \text{ kg/m}^3$.

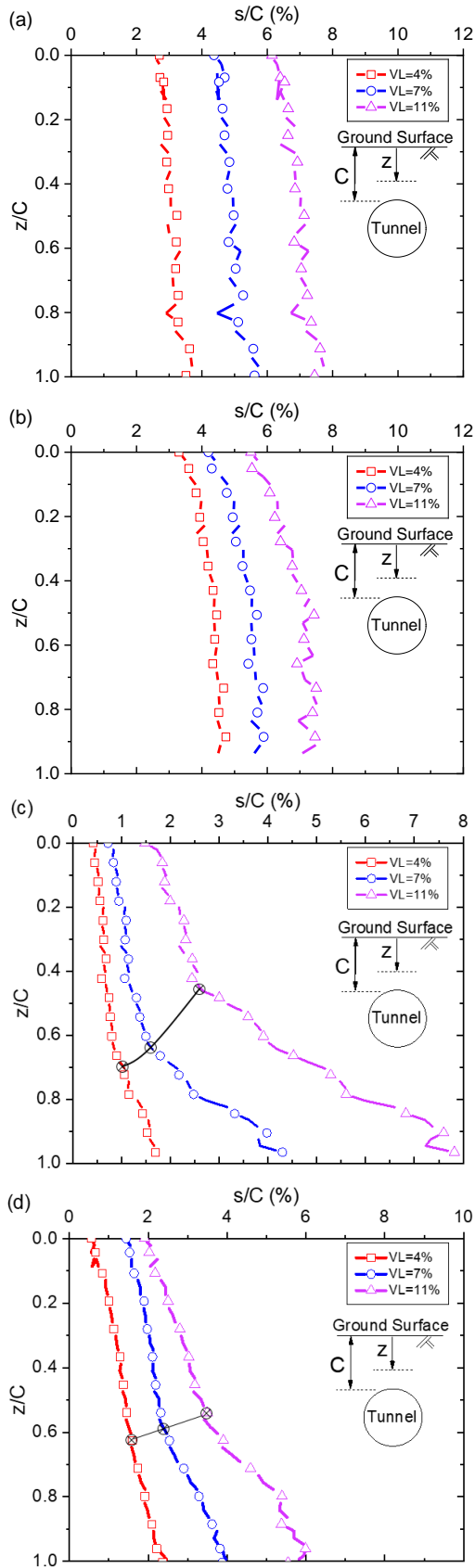


Figure 16. Variation of the vertical settlement above the tunnel crown for a cover-to-tunnel diameter ratio of $C/D=3$; (a) $\rho=1398$, (b) $\rho=1417$, (c) $\rho=1441$, (d) $\rho=1482$ kg/m^3 .

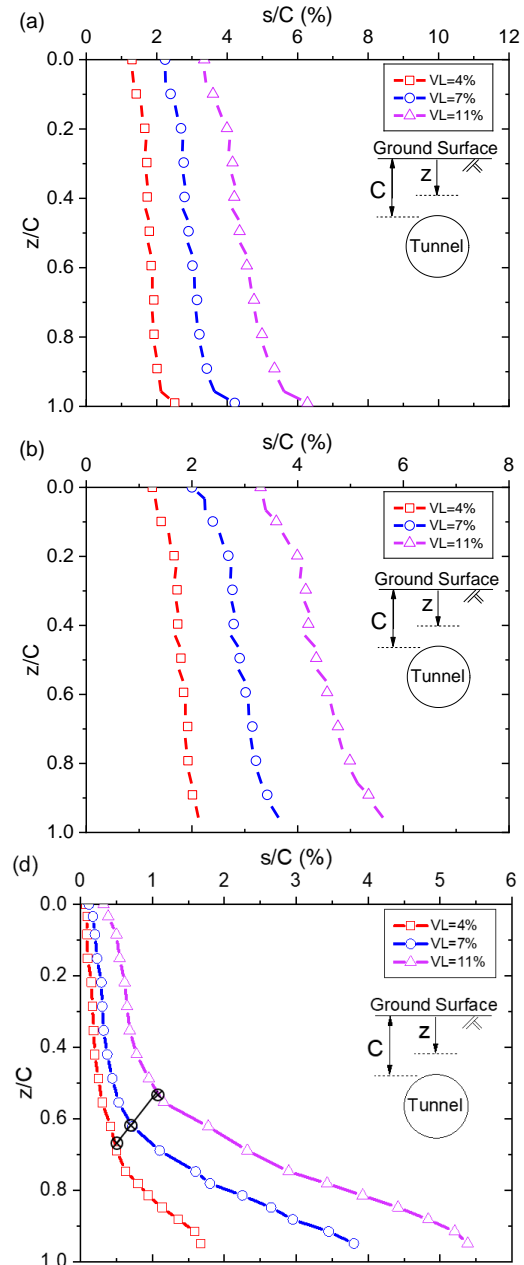


Figure 17. Variation of the vertical settlement above the tunnel crown for a cover-to-tunnel diameter ratio of $C/D=4$; (a) $\rho=1398$, (b) $\rho=1417$, (c) $\rho=1482$ kg/m^3 .

In this study, soil stress arching above the tunnel has been looked into from two aspects of being earth pressure measurement by miniature pressure cells and ground settlement by image processing. The height of inflection points observed in vertical earth pressure distribution (indicated in Figures 11-13), as well as the height of inflection points observed in-ground vertical settlement (indicated in Figures 15-17), are plotted in Fig.18 as a function of the cover-to-tunnel diameter ratio. Note that this figure is plotted for a tunnel volume loss of 7% where the height of the inflection point, defined as the height of the loosened zone (h), is normalized with tunnel diameter. A relatively good agreement can be seen between the data obtained from two different aspects of the investigation.

It is obvious from Figure 18 that the height of the loosened zone rises by increasing the cover-to-tunnel diameter ratio. Increasing the altitude of the loosened zone means extending the stress-released zone and applying higher pressure to the tunnel support system.

Based on the numerical analysis done by Lin et al. (2019), the height of the loosened zone for a tunnel with a cover-to-tunnel diameter ratio of 2 was estimated at $0.73D$, where D is the tunnel diameter. However,

according to this figure, the expecting height of the loosened zone for a cover-to-tunnel diameter ratio of 2 is about 1D (related to the 7% VL), which is close to what was estimated by Lin et al. (2019).

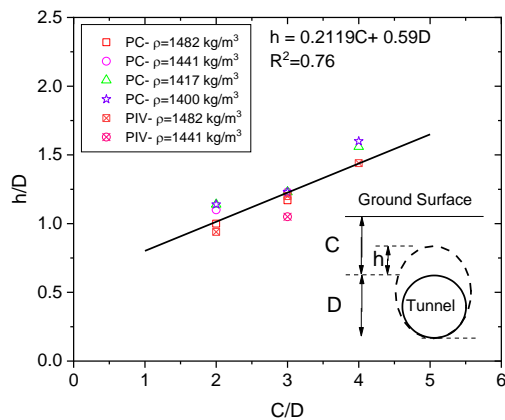


Figure 18. Normalized height of loosened zone (h/D) as a function of cover-to-tunnel diameter ratio (C/D) for a volume loss of 7%. (PC= data captured from pressure cells, PIV= data captured from image processing).

4. Conclusions

For the simulation of full-face circular shallow tunneling in sandy soils, a physical modeling setup was assembled. A series of physical models with different soil densities, cover-to-tunnel diameter ratios, and tunnel volume losses were conducted to investigate the development of stress arching above the tunnel. The variation in earth pressure was monitored by means of some miniature pressure cells. Particle Image Velocimetry was also used to measure the deformation of the model. The earth pressure measurement as well as image processing confirmed the development of soil arching, where an arching zone formed confining a loosened zone of soil above the tunnel. The results showed that the height of the loosened zone rises with increasing the cover-to-tunnel diameter ratio. Finally, through interpolation of physical data results of this study a linear equation was proposed for estimation of the height of the loosened zone as a function of the tunnel diameter and cover of the tunnel. As the weight of the loosened zone applies directly to the support system of the tunnel, estimation of this weight can help for a more effective and economical support system. However, this study was limited to cohesion less silica sand under loose conditions and more investigations on different types of soil are recommended.

Abbreviation

PIV, Particle Image Velocimetry; C/D , Cover-to-tunnel diameter ratio; h/D , the normalized height of the loosened zone; ρ , density.

REFERENCES

- [1] Balla, A. (1963). Rock pressure determined from shearing resistance'. Paper presented at the Proc. Int. Conf. Soil Mechanics, Budapest.
- [2] Chen, C. N., Huang, W. Y., & Tseng, C. T. (2011). Stress redistribution and ground arch development during tunneling. *Tunnelling and Underground Space Technology*, 26(1), 228-235. doi: <http://dx.doi.org/10.1016/j.tust.2010.06.012>
- [3] Chen, R. P., Li, J., Kong, L. G., & Tang, L. j. (2013). Experimental study on face instability of shield tunnel in sand. *Tunnelling and Underground Space Technology*, 33, 12-21. doi: <http://dx.doi.org/10.1016/j.tust.2012.08.001>
- [4] Fraldi, M., & Guarracino, F. (2010). Analytical solutions for collapse mechanisms in tunnels with arbitrary cross sections. *International Journal of Solids and Structures*, 47(2), 216-223. doi: <http://dx.doi.org/10.1016/j.jisolsolstr.2009.09.028>.
- [5] Handy, R. L. (1985). The arch in soil arching. *Journal of Geotechnical Engineering-Asce*, 111(3), 302-318.
- [6] I. Boonsiri, A., & Takemura, J. (2015). A Centrifuge Model Study on Pile Group Response to Adjacent Tunnelling in Sand. *Japan Society of Civil Engineers*, 3, 1-18.
- [7] Ibrahim, E., Soubra, A. H., Mollon, G., Raphael, W., Dias, D., & Reda, A. (2015). Three-dimensional face stability analysis of pressurized tunnels driven in a multilayered purely frictional medium. *Tunnelling and Underground Space Technology*, 49, 18-34. doi:10.1016/j.tust.2015.04.001
- [8] Katoh, Y., Miyake, M., & Wada, M. (1998). Ground deformation around shield tunnel. Paper presented at the Proceedings of the International Conference on Centrifuge Modelling (Centrifuge'98).
- [9] Khosravi, M. H., Pipatpongsa, T., & Takemura, J. (2013). Experimental analysis of earth pressure against rigid retaining walls under translation mode. *Geotechnique*, 63(12), 1020.
- [10] Khosravi, M. H., Pipatpongsa, T., Takahashi A. & Takemura, J. (2011). Arch action over an excavated pit in a stable scarp investigated by physical model tests. *Soil and foundations*, 51(4), 723-735.
- [11] Khosravi, M. H., Takemura, J., Pipatpongsa, T., & Amini, M. (2016). In-flight excavation of slopes with potential failure planes. *Journal of Geotechnical and Geoenvironmental Engineering*, 142(5), 06016001.
- [12] Kirsch, A. (2010). Experimental investigation of the face stability of shallow tunnels in sand. *Acta Geotechnica*, 5(1), 43-62.
- [13] Kirsch, G. (1898). Theory of elasticity and application in strength of materials. *Zeitschrift des Vereins Deutscher Ingenieure*, 42(29), 797-807.
- [14] Krynine, D. P. (1945). Discussion of "Stability and Stiffness of Cellular Cofferdams". *Transactions of the American Society of Civil Engineers*, 10(1), 1175-1178.
- [15] Lei, M., Peng, L., & Shi, C. (2015). Model test to investigate the failure mechanisms and lining stress characteristics of shallow buried tunnels under unsymmetrical loading. *Tunnelling and Underground Space Technology*, 46, 64-75. doi: <http://dx.doi.org/10.1016/j.tust.2014.11.003>
- [16] Lin, X. T., Chen, R. P., Wu, H. N., & Cheng, H. Z. (2019). Three-dimensional stress-transfer mechanism and soil arching evolution induced by shield tunneling in sandy ground. *Tunnelling and Underground Space Technology*, 93, 103104. doi: <https://doi.org/10.1016/j.tust.2019.103104>.
- [17] Marshall, A., Farrell, R., Klar, A., & Mair, R. (2012). Tunnels in sands: the effect of size, depth and volume loss on greenfield displacements. *Geotechnique*, 62(5), 385.
- [18] Marston, A., & Anderson, A. (1913). The theory of loads on pipes in ditches and tests on cement and clay drain tile and sewer pipe (Vol. 31). *Bulletins of the Engineering Experiment*.
- [19] Mollon, G., Dias, D., & Soubra, A. H. (2011). Rotational failure mechanisms for the face stability analysis of tunnels driven by a pressurized shield. *International Journal for Numerical and Analytical Methods in Geomechanics*, 35(12), 1363-1388.
- [20] Moussaei, N., Khosravi, M. H., & Hossaini, M. F. (2019). Physical modeling of tunnel induced displacement in sandy grounds. *Tunnelling and Underground Space Technology*, 90, 19-27.

- [21] Moussaei, N., Sharifzadeh, M., Sahriar, K., & Khosravi, M. H. (2019). A new classification of failure mechanisms at tunnels in stratified rock masses through physical and numerical modeling. *Tunnelling and Underground Space Technology*, 91, 103017.
- [22] Moussaei, N., Sharifzadeh, M., Shahriar, K., & Khosravi, M. (2016). Evaluation of discontinuity and opening geometry effects on roof beam deflection. Paper presented at the ISRM International Symposium-EUROCK 2016.
- [23] Moussaei, N., Sharifzadeh, M., Sahriar, K., & Khosravi, M. H. (2018). On Stability of Shallow Tunnel by Model Test and Numerical Simulation. Paper presented at the Proceedings of China-Europe Conference on Geotechnical Engineering.
- [24] Pan, Q., & Dias, D. (2017). Upper-bound analysis on the face stability of a non-circular tunnel. *Tunnelling and Underground Space Technology*, 62, 96-102. doi: <http://dx.doi.org/10.1016/j.tust.2016.11.010>.
- [25] Rezaei, M., Hossaini, M. F., Majdi, A., & Najmoddini, I. (2017). Determination of the height of distressed zone above the mined panel: An ANN model. *International Journal of Mining and Geo-Engineering*, 51(1), 1-7.
- [26] Svein, J. K. (2004). An introduction to MatPIV v. 1.6. 1. Preprint series. *Mechanics and Applied Mathematics* Error! Hyperlink reference not valid.. nb. no/URN: NBN: no-23418.
- [27] Terzaghi, K. (1936). Stress distribution in dry and saturated sand above a yielding trap-door. Paper presented at the The First International Conference on Soil Mechanics and Foundation Engineering, Harvard University, Cambridge.
- [28] Terzaghi, K. (1943). *Arching in ideal soils Theoretical soil mechanics*. New York: Wiley.
- [29] Yang, X. L., Yang, Z. H., Li, Y. X., & Li, S. C. (2013). Upper bound solution for supporting pressure acting on shallow tunnel based on modified tangential technique. *Journal of Central South University*, 20(12), 3676-3682. doi:10.1007/s11771-013-1895-y
- [30] Zhang, C., Han, K., & Zhang, D. (2015). Face stability analysis of shallow circular tunnels in cohesive–frictional soils. *Tunnelling and Underground Space Technology*, 50, 345-357. doi: <http://dx.doi.org/10.1016/j.tust.2015.08.007>.